ISSN 1063-7826, Semiconductors, 2013, Vol. 47, No. 5, pp. 606–611. © Pleiades Publishing, Ltd., 2013.
Original Russian Text © I.E. Tyschenko, V.A. Volodin, M. Voelskow, A.G. Cherkov, V.P. Popov, 2013, published in Fizika i Tekhnika Poluprovodnikov, 2013, Vol. 47, No. 5, pp. 591–596.

SURFACES, INTERFACES, AND THIN FILMS

Crystallization Induced by Thermal Annealing with Millisecond Pulses in Silicon-on-Insulator Films Implanted with High Doses of Hydrogen Ions

I. E. Tyschenko[a]^, V. A. Volodin[b], M. Voelskow[c], A. G. Cherkov[a], and V. P. Popov[a]

[a] *A.V. Rzhanov Institute of Semiconductor Physics, Siberian Branch, Russian Academy of Sciences, Novosibirsk, 630090 Russia*
^e-mail: tys@isp.nsc.ru
[b] *Novosibirsk State University, Novosibirsk, 630090 Russia*
[c] *Institute of Ion-Beam Physics and Materials Research, Dresden, 01328 Germany*

Submitted June 25, 2012; accepted for publication July 2, 2012

Abstract—The crystallization of silicon-on-insulator films, implanted with high doses of hydrogen ions, upon annealing with millisecond pulses is studied. Immediately after hydrogen-ion implantation, the formation of a three-phase structure composed of silicon nanocrystals, amorphous silicon, and hydrogen bubbles is detected. It is shown that the nanocrystalline structure of the films is retained upon pulsed annealing at temperatures of up to ~1000°C. As the temperature of the millisecond annealing is increased, the nanocrystal dimensions increase from 2 to 5 nm and the fraction of the nanocrystalline phase increases to ~70%. From an analysis of the activation energy of crystal phase growth, it is inferred that the process of the crystallization of silicon films with a high (~50 at %) hydrogen content is limited by atomic-hydrogen diffusion.

DOI: 10.1134/S1063782613050229

1. INTRODUCTION

The production of high-efficiency thin-film solar cells is a rather prospective task, requiring the development of novel materials to provide both greater opportunities for solar-light conversion and a high degree of tolerance to long-term irradiation. In this respect, heterophase nanocrystalline silicon consisting of silicon nanocrystals separated by an amorphous interlayer is attracting much attention [1, 2]. Heterophase nanocrystalline silicon layers have a number of advantages over amorphous silicon, which is widely used for the production of low-cost thin-film photovoltaic devices [3]. First of all, the two-phase structure provides the efficient absorption of light in a wider spectral region. In this case, short-wavelength radiation (in the blue and green spectral regions) is absorbed in amorphous silicon, whereas long-wavelength radiation (in the red and orange regions) is absorbed in silicon nanocrystals. In other words, nanocrystalline silicon absorbs light in practically the entire visible and near-infrared region of the energy spectrum (down to 1.1 eV). Another advantage of such a material is its high stability to solar radiation compared to that of amorphous silicon [4, 5].

The properties of heterophase nanocrystalline silicon are defined in many respects by the grain size, the content of the crystal phase, and the state of the interface between the grains and surrounding amorphous matrix [6]. At the same time, an important role is played by the structure of the amorphous silicon separating the nanocrystalline islands. Specifically, the content and position of hydrogen atoms in the amorphous silicon interlayer is an important factor. Hydrogen atoms are capable of forming stable Si–H bonds in silicon at temperatures below 300°C by interacting with dangling bonds as well as by being incorporated into strained Si–Si bonds, thus stimulating the crystallization of amorphous silicon [7]. However, at temperature above 300°C, the Si–H bonds break, atomic hydrogen is released, and H_2 molecules are formed. These molecules are further capable of accumulating in hollow microspaces to form hydrogen bubbles. Structural transformations in silicon with the participation of hydrogen bubbles are commonly considered in studies of the hydrogen-assisted cleaving of single-crystal semiconductor layers [8]. Virtually no data on the influence of the state of hydrogen in silicon films upon the crystallization of amorphous silicon are available in published works. In this study, we investigate the process of the crystallization of thin amorphous silicon films containing a large proportion of hydrogen upon annealing with millisecond pulses. Hydrogen-containing silicon films were formed by implanting silicon-on-insulator (SOI) layers with high hydrogen-ion doses, providing a hydrogen content at a level of 50 at %.

2. EXPERIMENTAL

For the initial material, we used SOI wafers with a thickness of the cut-off silicon layer of 280 nm and

thickness of the buried silicon-oxide layer of 400 nm. The *p*-Si wafers were oriented in the (100) direction. Hydrogen ions with an energy of 24 keV and dose of 5×10^{17} cm^{-2} were implanted from the pulsed plasma ion source using a system developed at the Budker Institute of Nuclear Physics, Siberian Branch, Russian Academy of Sciences. According to calculations using the TRIM software, the above ion parameters were expected to provide an atomic hydrogen content in the film of ~50 at %. Subsequent heat treatment of the films was conducted with a xenon lamp at temperatures of 600–1000°C for a duration of 20 ms at the Institute of Ion-Beam Physics and Materials Research, Helmholtz-Zentrum Dresden-Rossendorf, Dresden (Germany). During pulse annealing, the structures were steadily heated to a temperature of 550°C with the use of a halogen lamp. Annealing was conducted in an argon atmosphere. For comparison, we studied the corresponding structures annealed in a nitrogen atmosphere in a furnace at temperatures of 200–1000°C for a duration of 20 min. The structural properties of the formed samples were studied by transmission electron microscopy (TEM). TEM analysis was carried out with a JEM-4000 microscope operating with a resolution of 0.2 nm, at an accelerating voltage of 250 kV. As another method of studying the structural properties of the initial and annealed samples, we used Raman spectroscopy. The Raman spectra were excited with Ar laser radiation at the wavelength 514.5 nm. The power incident on the sample was 2–3 mW. The Raman measurements were conducted at room temperature. The probe spot was 6–8 μm in size. For the measurements, we used a spectrometer with a T64000 Horiba Jobin Yvon triple monochromator. The spectral resolution of the spectrometer was no worse than 2 cm^{-1}. A silicon matrix of photodetectors cooled with liquid nitrogen served as the detector. The measurements were carried out in the backscattering experimental geometry; the polarization vector of the incident light was parallel to the $\langle 011 \rangle$ crystallographic direction of silicon. The scattered light was recorded for the $\langle 01\bar{1} \rangle$ polarization. The chosen geometric layout of measurements allowed maximum suppression of the Raman signal from the silicon substrate.

3. RESULTS AND DISCUSSION

Figure 1 shows the TEM image of the surface of the SOI structure immediately after implantation with hydrogen ions. From Fig. 1, it can be seen that, even immediately after implantation, hydrogen bubbles are formed on the surface of the SOI layer, and the bubble diameter varies in the range from 100 to 1000 nm. The bubbles have a dome-like shape, with the maximum dome height reaching 600 nm (see inset in Fig. 1). As the annealing temperature is elevated, the dome sizes vary nonmonotonically.

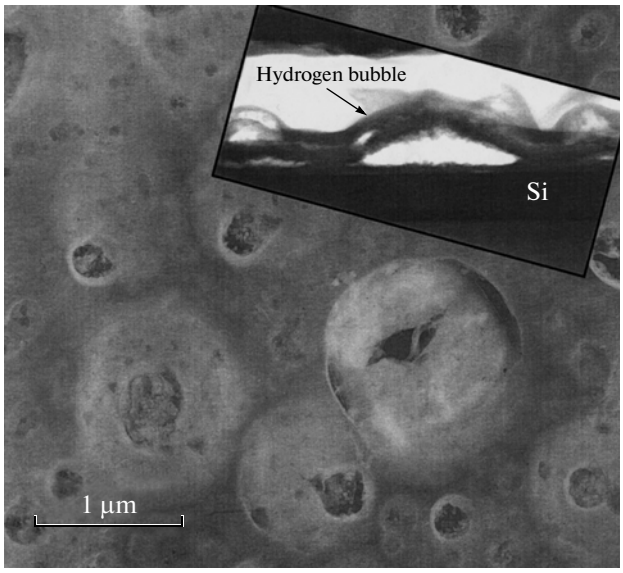

Fig. 1. TEM image of the surface of the SOI film implanted with hydrogen ions with the energy 24 keV and the dose 5×10^{17} cm^{-2}. The inset shows a TEM image of an individual hydrogen bubble on the surface of the SOI layer, as obtained for the transverse section.

Figure 2 shows the Raman spectra recorded for hydrogen-ion-implanted SOI films before and after pulse annealing at temperatures of $T_a = 600$–1000°C. In the spectra of the unannealed SOI structures, a peak observed at about 472 cm^{-1} is dominant. This peak position corresponds to the transverse optical (TO) phonon frequency in hydrogenated amorphous silicon [9]. At about 514 cm^{-1}, we observe some asymmetry in the form of a slightly pronounced shoulder. The full width at half maximum (FWHM) of the peak related to amorphous silicon is about 70 cm^{-1}. After annealing at 600°C, the intensity of this peak is found to be about two times lower, and the shoulder observed in the high-frequency region is transformed into a clearly pronounced peak at about 516 cm^{-1}. The observed peak is due to scattering at optical phonons localized in the silicon nanocrystals. An increase in the annealing temperature to 800°C is accompanied by a further shift of this peak to high frequencies (518 cm^{-1}) and by a steady increase in its intensity. On annealing at temperatures above 800°C, the frequency of the localized optical mode remains unchanged; only an increase in its intensity and a decrease in the FWHM are observed. The inset in Fig. 2 shows the Raman spectra of bulk single-crystal silicon and of the implanted SOI structures annealed at 1000°C for 20 ms. It can be seen that, even after high-temperature annealing, the intensity of the Raman peak remains three times lower than that for single-crystal silicon and the peak is shifted to lower frequencies. In addition, the 518 cm^{-1} peak is two times larger in width than the optical-phonon peak in single-crystal silicon.

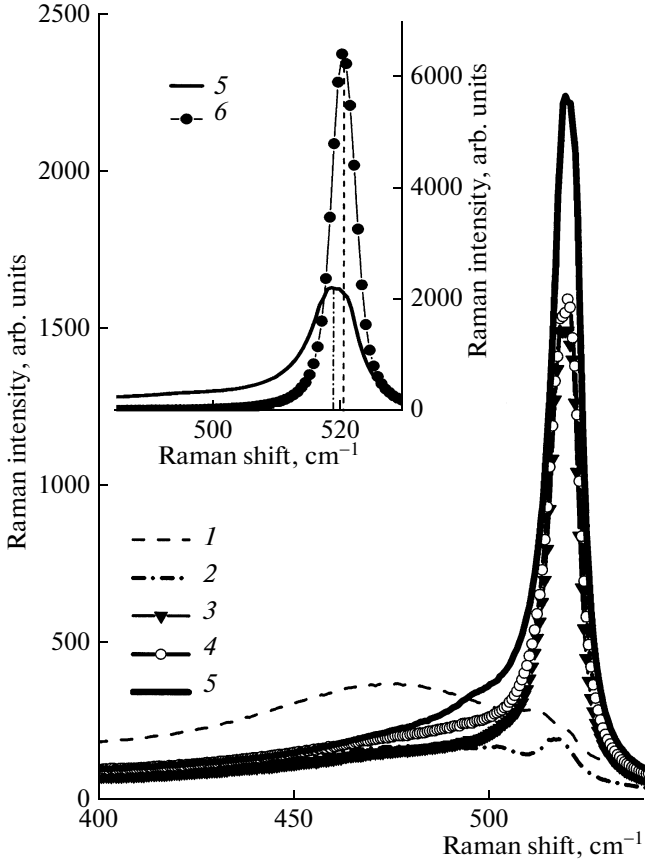

Fig. 2. Raman spectra recorded for the hydrogen-ion-implanted SOI films (*1*) before and (*2*) after 20-ms pulse annealing at the temperatures T_a = (*2*) 600, (*3*) 800, (*4*) 900, and (*5*) 1000°C. Curve *6* refers to the Raman spectrum of single-crystal silicon.

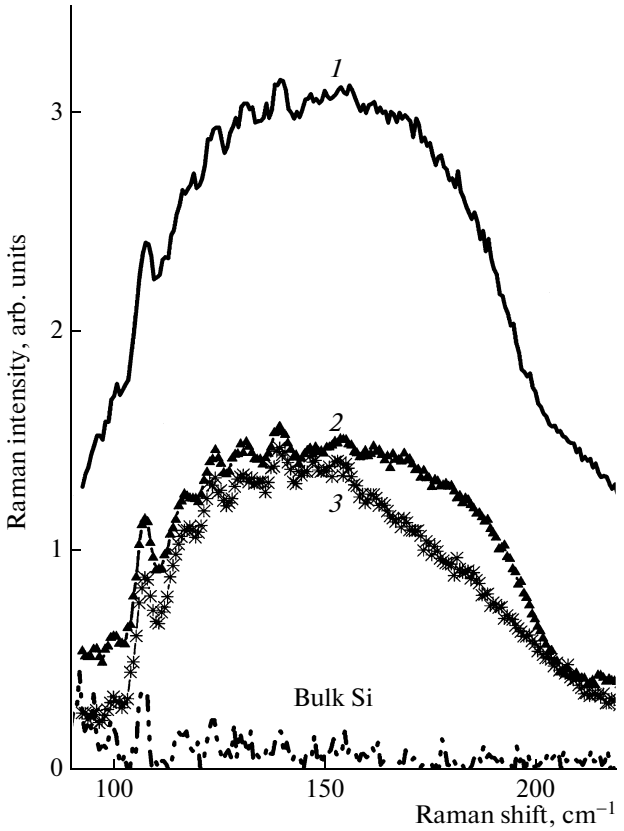

Fig. 3. Raman spectra recorded in the range 90–220 cm^{-1} for the SOI films implanted with hydrogen ions with the energy 24 keV and the dose 5×10^{17} cm^{-2}. The spectra are recorded (*1*) before and (*2*, *3*) after 20-ms pulse annealing at the temperatures T_a = (*2*) 600 and (*3*) 1000°C.

These data suggest that, in the films subjected to pulse annealing, a high degree of localization of optical phonons is retained. This can be due to both the presence of silicon nanocrystals and a rather high degree of disorder in the film. It should be noted that the amorphous component remains rather noticeable even after millisecond annealing at 1000°C (inset in Fig. 2).

More comprehensive data on the structural transformations in hydrogenated amorphous silicon can be gained from an analysis of low-frequency Raman spectra defined by scattering at acoustic phonons [10, 11]. Figure 3 shows the low-frequency Raman spectra of the SOI films implanted with a high dose of hydrogen ions; the spectra were recorded before and after annealing of the films at temperatures of 600 and 1000°C for 20 ms. In addition, Figure 3 shows the low-frequency Raman spectra of bulk single-crystal silicon. From Fig. 3, it can be seen that, immediately after implantation, a broad high-intensity band with a peak at 150 cm^{-1} is observed in the spectra. A series of narrow peaks in the low-frequency spectral region corresponds to Raman scattering at the vibrational–rotational modes of nitrogen and oxygen molecules in the atmosphere. The frequency position of the above-mentioned 150 cm^{-1} peak corresponds to the transverse acoustic phonon frequency at the boundary of the Brillouin zone of the silicon lattice. In single-crystal silicon, this peak is not observed, since the translation symmetry in the bulk crystal yields the selection rules prohibiting Raman scattering at phonons in this spectral region. Defect generation often violates the translation symmetry and removes the prohibition imposed by the selection rules, which is accompanied by enhancement of Raman scattering at acoustic phonons with a large wave number and, correspondingly, a high frequency. As is evident from Fig. 3, millisecond annealing at 600°C decreases the intensity of the Raman band more than twofold. This is indicative of the annealing of structural imperfections in the regions of implanted silicon. However, a further increase in the annealing temperature up to 1000°C is not accompanied by corresponding changes in the intensity of the Raman peak, but induces only a slight decrease in the width of this peak. Similar spectra were also recorded for the samples annealed at temperatures 200–1000°C for 20 min. Figure 4 shows the

dependence of the logarithm of the change in the relative area of the ~150-cm^{-1} Raman peak upon the inverse temperature of pulse annealing (experimental data approximated by line *2*) and conventional annealing in a furnace (experimental data approximated by line *1*). It can be seen that, in the case of conventional annealing, the change in the area of the low-frequency Raman peak in the entire temperature range can be approximated by a straight line with a slope corresponding to the activation energy 0.134 eV; this energy exactly corresponds to the activation energy of the structural transformations of dangling bonds saturated with hydrogen atoms [12, 13]. In the case of millisecond annealing at temperatures of ~600°C and higher, the structural transformations responsible for changes in the optical-phonon spectrum in silicon have no effect upon the acoustic-phonon spectra. This means that millisecond-pulse annealing of silicon films with a high hydrogen content does not induce any translation symmetry, even if the annealing temperature is about 1000°C.

Thus, the TEM and Raman data show that, in silicon films implanted with high doses of H^+ ions, hydrogen bubbles and silicon nanocrystals are formed. The nanocrystals create conditions for the confinement of phonon wave functions within the nanocrystal bulk. In this case, the order of a localized phonon mode is defined by the number of half-wavelengths, which is a multiple of the crystal size. Because of the dispersion relation for optical phonons, their frequency decreases with decreasing wavelength. Therefore, a decrease in the nanocrystal dimensions is accompanied by a shift of the peak related to TO phonons to lower frequencies in the Raman spectrum. The phenomenological relation that allows one to establish a relationship between the frequency shift of the first-order localized mode ω_{nc} with respect to the frequency of long-wavelength optical vibrations in bulk silicon ω_{Si} and the silicon nanocrystal size D_{nc} can be written as [14]

$$\Delta\omega = \omega_{Si} - \omega_{nc} = B\left(\frac{a}{D_{nc}}\right)^{\gamma}. \quad (1)$$

Here, $a = 0.543$ nm is the lattice constant of silicon. The parameters B and γ depend on the shape of the nanocrystal. In the calculations carried out in the context of the bond polarizability model for the frequencies of optical modes localized in spherically shaped nanocrystals [15], these parameters are $B = 47.41$ cm^{-1} and $\gamma = 1.44$. Figure 5 shows the silicon nanocrystal diameter calculated by expression (1) versus the temperature of the postimplantation annealing of the implanted SOI films, for the cases of millisecond annealing and thermal annealing for 20 min. It can be seen that, after steady-state annealing, the SOI films are almost completely crystallized even at temperatures of about 900°C; however, after pulsed annealing, the films remain nanocrystalline up to a temperature

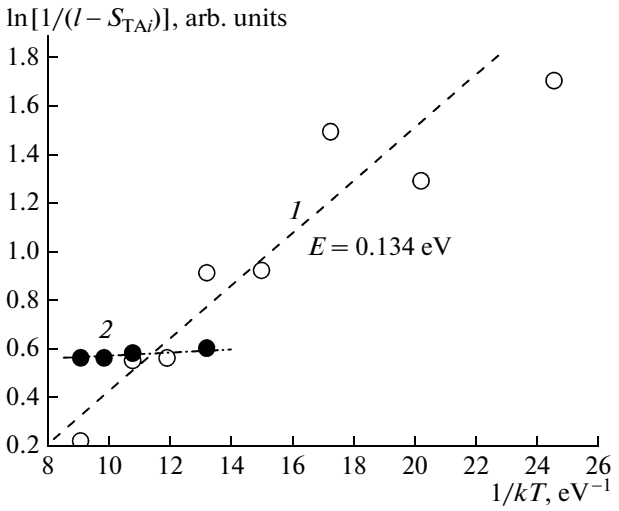

Fig. 4. Logarithm of the change in the relative area of the 150-cm^{-1} Raman peak versus the inverse temperature of annealing for (*1*) 20 min and (*2*) 20 ms.

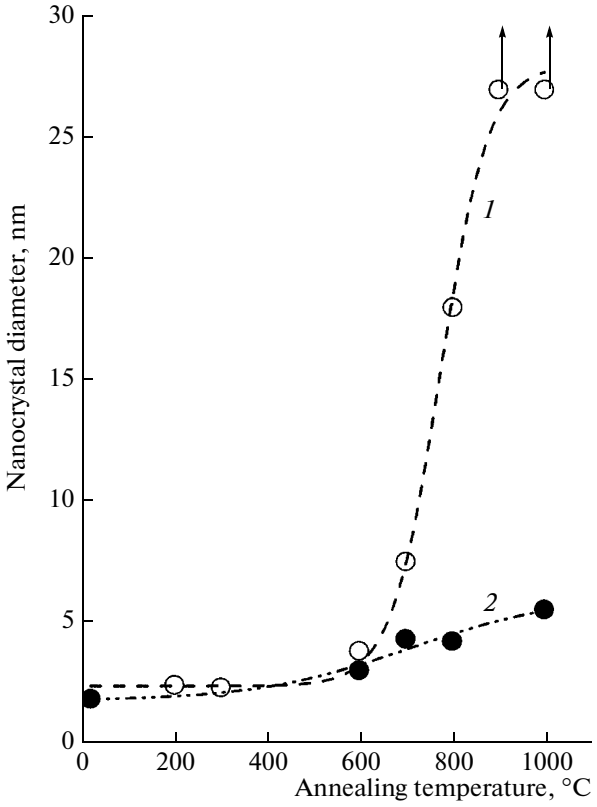

Fig. 5. Silicon nanocrystal diameter calculated by expression (1) versus the temperature of postimplantation annealing for (*1*) 20 min and (*2*) 20 ms for the SOI films implanted with hydrogen ions with the energy 24 keV and the dose 5×10^{17} cm^{-2}.

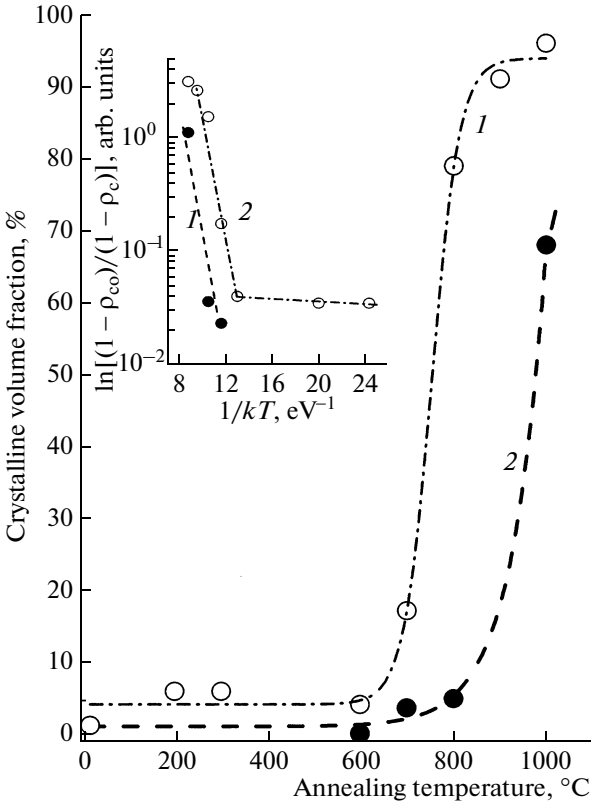

Fig. 6. Volume fraction of the crystalline phase in the SOI films implanted with hydrogen ions with the energy 24 keV and the dose 5×10^{17} cm^{-2} versus the temperature of postimplantation annealing for (*1*) 20 min and (*2*) 20 ms. The inset shows the corresponding dependences of the fraction of the crystalline phase on the inverse temperature, as calculated in accordance with Avrami's formula.

of 1000°C. In this case, the size of the nanocrystal does not exceed 5 nm.

Quantitative analysis of the Raman spectra in the region of optical phonon frequencies allows us to determine the volume fractions of the amorphous and crystalline components of the synthesized films. For example, the crystalline fraction ρ_c can be expressed as [16]

$$\rho_c = \frac{I_c}{I_c + yI_a}. \quad (2)$$

Here, I_c and I_a are the corresponding integrated Raman intensities for scattering in the crystalline and amorphous phases and $y = \Sigma_c/\Sigma_a$, where Σ_c and Σ_a are the integrated backscattering cross sections in the spectral region of interest for crystalline and amorphous silicon, respectively. The integrated Raman cross section related to the TO phonon is a function of the nanocrystal size D_{nc} (expressed in nanometers) [16]:

$$y = 0.1 + \exp\left(\frac{-D_{nc}}{25}\right). \quad (3)$$

Using the data of Fig. 5 and expressions (2) and (3), we have determined the volume fraction of the crystalline phase as a function of the temperature of pulse and steady-state annealing. The integrated intensities were determined by decomposing the experimental Raman spectra into Gaussian or Lorentzian components and subsequently integrating them. The results are shown in Fig. 6. From this figure, it can be seen that the crystallization of SOI films with high hydrogen proportions upon annealing with millisecond pulses is moderated compared to crystallization upon conventional thermal annealing. According to the results obtained here, the nanocrystalline fraction of the SOI films implanted with high doses of hydrogen ions and annealed in the pulse mode can be as high as 70%.

We now discuss how the process of the crystallization of silicon films implanted with high doses of hydrogen ions depends on the annealing time. From Fig. 6, it is evident that, in silicon with a high content of hydrogen, the crystalline phase grows only at temperatures higher than 600°C. In this case, the crystallization process can be described by Avrami's formula [17, 18]

$$\ln\left[\frac{1-\rho_{c0}}{1-\rho_c}\right] = -A\exp\left(\frac{-E_a}{kT}\right). \quad (4)$$

Here, ρ_{c0} is the volume fraction of the crystalline phase in the unannealed films, E_a is the crystallization activation energy, k is the Boltzmann constant, $A = (\nu t)^m$ is the pre-exponential factor dependent on the annealing time t and the frequency factor ν, and the value of m varies between 3 and 4 [17]. The inset in Fig. 6 shows the dependences of the volume fraction of the crystalline phase on the inverse temperature in the coordinates $\ln[(1 - \rho_{c0})/(1 - \rho_c)]$ and $1/kT$ for the corresponding films annealed under conditions of millisecond annealing and for the films annealed for 20 min. It can be seen that, in both cases, the dependences exhibit identical slopes. This means that, upon pulse and steady-state annealing, the crystallization activation energies are controlled by the same processes and differ only in terms of the value of the pre-exponential factor A involving the annealing time. The process consists of two stages. The first (low-temperature) stage proceeds at temperatures below 600°C, with an activation energy of ~0.01 eV. In hydrogenated amorphous silicon, in which the hydrogen content is no higher than 10 at %, the above-mentioned low-temperature stage commonly proceeds with an activation energy that is two orders of magnitude higher than the above-indicated energy and is controlled by the structural transformations of dangling bonds, including those saturated with hydrogen atoms [13]. This statement is also consistent with the data of Fig. 3, in which it is shown that the activation energy of the 20-min isochronous annealing of defects responsible for the acoustic mode in the Raman spectrum of silicon is close to 0.1 eV. The above-indicated difference between the experimental crystallization activation energies suggests that, in films with high hydrogen

fractions, structural transformations of dangling bonds saturated with hydrogen atoms are not the factor that limits the crystallization process.

The activation energy that describes the high-temperature stage of crystallization (see Fig. 6) in the case under consideration substantially differs from the well-known activation energy of heterogeneous solid-phase crystallization (2.8–4.7 eV [19]). The activation energy estimated here at 1.5 eV coincides with the activation energy of the diffusion of atomic hydrogen in amorphous silicon. This can mean that, in the silicon films implanted with high doses of hydrogen, the crystalline phase grows through the ordering of strained Si–Si bonds due to the diffusion of atomic hydrogen from hydrogenated amorphous silicon regions separating crystalline nanoregions, rather than through a phase transition from the amorphous state to the crystalline state. In this case, a decrease in the annealing time is favorable for slowing down the release of hydrogen from the implanted region of the film. In accordance with expression (4), this effect shifts the activation dependence to higher temperatures. This means that complete crystallization of the silicon films upon pulse annealing occurs at temperatures higher than the crystallization temperatures for conventional steady-state annealing. In the case of pulse annealing even at temperatures of up to 1000°C, silicon nanocrystals are retained in the form of single-crystal silicon islands separated by a hydrogenated amorphous silicon interlayer. After pulse high-temperature annealing, the films present a texture that consists of oriented nanocrystals separated by a thin amorphous interlayer. In this case, the position of the Raman peak related to scattering at optical phonons is defined by the size of individual nanocrystalline grains forming the texture rather than by the size of the nanotextured regions.

Thus, in the study of SOI films implanted with high doses of hydrogen ions, providing a 50% hydrogen content, the formation of a three-phase system consisting of hydrogen bubbles, hydrogenated amorphous silicon, and silicon nanocrystals is observed. As the temperature of postimplantation millisecond-pulse annealing is elevated, hydrogenated amorphous silicon crystallizes, which is accompanied by growth of the nanocrystalline phase. The nanocrystalline structure of the layers is retained at temperatures of up to ~1000°C. As the temperature is increased, the nanocrystals increase in dimensions from 2 to 5 nm, and the fraction of the nanocrystalline phase increases to ~70%. The activation energy of growth of the crystalline phase is 1.5 eV, which corresponds to the activation energy of the diffusion of atomic hydrogen in hydrogenated amorphous silicon.

ACKNOWLEDGMENTS

We are grateful to I.I. Morozov for carrying out the hydrogen-ion implantation. The studies were carried out with the use of analytical equipment of the Center of Collective Use of the Research and Education Complex “Nanosystems and Advanced Materials”, Novosibirsk State University.

REFERENCES

1. B. Yan, G. Yue, J. M. Owens, J. Yang, and S. Guha, Appl. Phys. Lett. **85**, 1925 (2004).
2. R. Biswas and C. Xu, Opt. Express **19**, A664 (2011).
3. B. Rech and H. Wagner, Appl. Phys. A **69**, 155 (1999).
4. A. Chowdhury, S. Mukhopadhyay, and S. Ray, Solar Energy Mater. Solar Cells **93**, 597 (2009).
5. S. Mukhopadhyay, R. Goswami, and S. Ray, Solar Energy Mater. Solar Cells **93**, 674 (2009).
6. S. Klein, F. Finger, R. Carius, T. Dylla, B. Rech, M. Grimm, L. Houben, and M. Stutzmann, Thin Solid Films **430**, 202 (2003).
7. M. S. Valipa, S. Sriraman, E. S. Aydil, and D. Maroudas, J. Appl. Phys. **100**, 053515 (2006).
8. Q.-Y. Tong, K. Gutjahr, S. Hopfe, U. Gösele, and T.-H. Lee, Appl. Phys. Lett. **70**, 1390 (1997).
9. F. A. Sarrot, Z. Iqbal, and S. Veprek, Solid State Commun. **42**, 465 (1982).
10. A. P. Sokolov, A. P. Shebanin, O. A. Golikova, and M. M. Mezdrogina, J. Phys.: Condens. Matter **3**, 9887 (1991).
11. N. N. Ovsyuk and V. N. Novikov, Phys. Rev. **57**, 14615 (1998).
12. N. H. Nickel and E. A. Schiff, Phys. Rev. B **58**, 1114 (1998).
13. D. T. Britton, A. Hempel, M. Harting, G. Kogel, P. Sperr, W. Triftshauser, C. Arendse, and D. Knoesen, Phys. Rev. B **64**, 075403 (2001).
14. G. Faraci, S. Gibilisco, P. Russo, and A. Pennisi, Phys. Rev. B **73**, 033307 (2006).
15. J. Zi, H. Büscher, C. Falter, W. Ludwig, K. Zhang, and X. Xie, Appl. Phys. Lett. **69**, 200 (1996).
16. E. Bustarret, M. A. Hachicha, and M. Brunel, Appl. Phys. Lett. **52**, 1675 (1988).
17. J. Gonzalez-Hermandez and R. Tsu, Appl. Phys. Lett. **42**, 90 (1983).
18. T. Okada, T. Iwaki, H. Kasahara, and K. Yamamoto, Solid State Commun. **52**, 363 (1984).
19. U. Köstner, Phys. Status Solidi A **48**, 313 (1978).

Translated by E. Smorgonskaya